SUPPORTING INFORMATION

Magnetically sensitive light-induced reactions in cryptochrome are consistent with its proposed role as a magnetoreceptor

Kiminori Maeda[a,1], Alexander J. Robinson[a,1], Kevin B. Henbest[a], Hannah J. Hogben[b], Till Biskup[b], Margaret Ahmad[c], Erik Schleicher[d], Stefan Weber[d], Christiane R. Timmel[a,2] & P. J. Hore[b,2]

[a]Department of Chemistry, University of Oxford, Centre for Advanced Electron Spin Resonance, Inorganic Chemistry Laboratory, Oxford, UK.

[b]Department of Chemistry, University of Oxford, Physical & Theoretical Chemistry Laboratory, Oxford, UK.

[c]Université Paris VI, 4 Place Jussieu, 75005 Paris, France and Pennsylvania State University, Media, Pennsylvania 19063, USA.

[d]Institute of Physical Chemistry, Albert-Ludwigs-Universität Freiburg, 79104 Freiburg, Germany.

[1]These authors contributed equally to this work.

[2]To whom correspondence may be addressed. E-mail: peter.hore@chem.ox.ac.uk or christiane.timmel@ chem.ox.ac.uk

Contents

1. Magnetic field effects on radical kinetics
2. Flavin–tryptophan photoreaction mechanism
3. Correlation between the magnetic field effect on the yield of RP2 and the lifetime of RP1 in *Ec*PL.
4. Calculation of $B_{1/2}$
5. Simulation of magnetic field effects

1. Magnetic field effects on radical kinetics

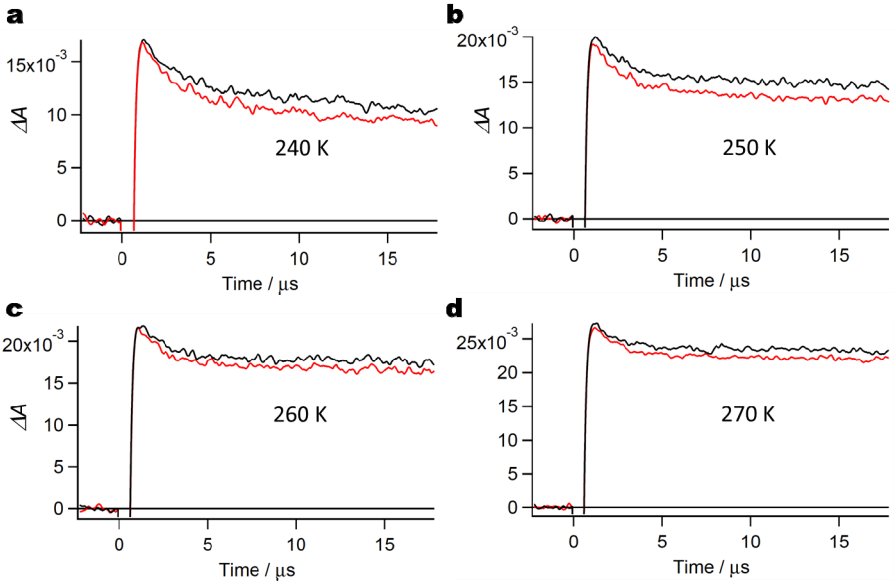

Fig. S1. Transient absorption kinetic time profiles of *Ec*PL recorded at 510 nm in 50% glycerol solution with (red) and without (black) a 28 mT applied magnetic field at the temperatures indicated. Results were obtained as the average of 10 laser shots, with 200 ns boxcar smoothing.

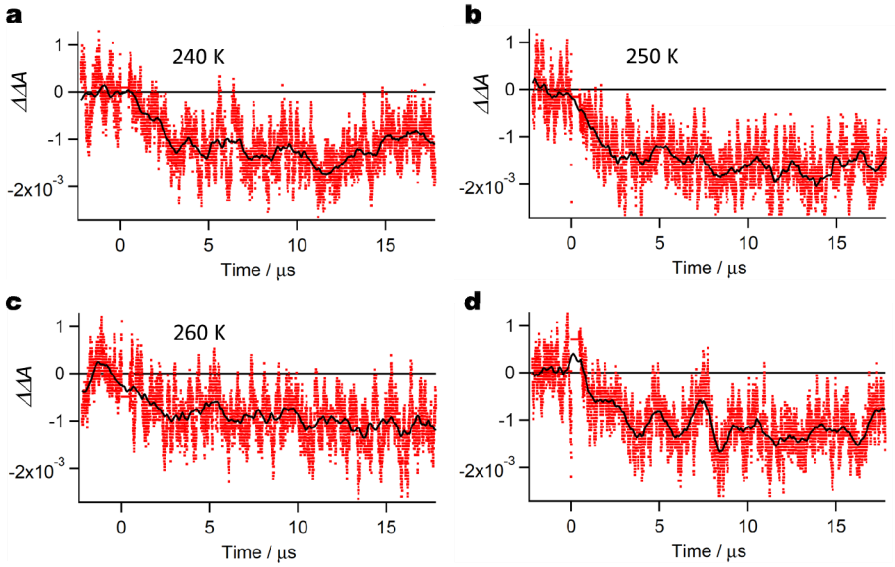

Fig. S2. Difference signals calculated from the data in Fig. S1: $\Delta\Delta A = \Delta A(28\ \text{mT}) - \Delta A(0)$. Red dots represent raw, unsmoothed data; black lines represent the same data after 1 μs boxcar smoothing.

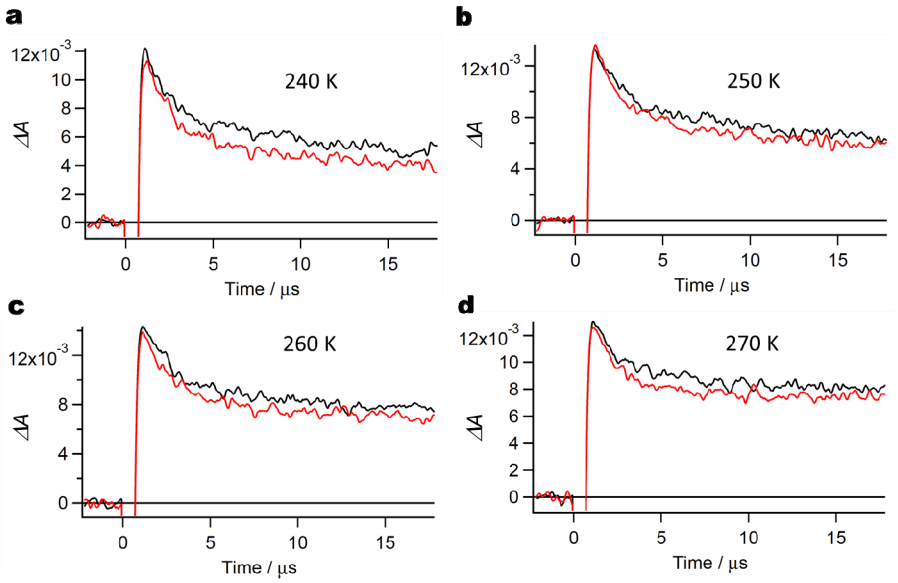

Fig. S3. Transient absorption kinetic time profiles of *Ec*PL recorded at 510 nm in 65% glycerol solution with (red) and without (black) a 28 mT applied magnetic field at the temperatures indicated. Results were obtained as the average of 10 laser shots, with 200 ns boxcar smoothing.

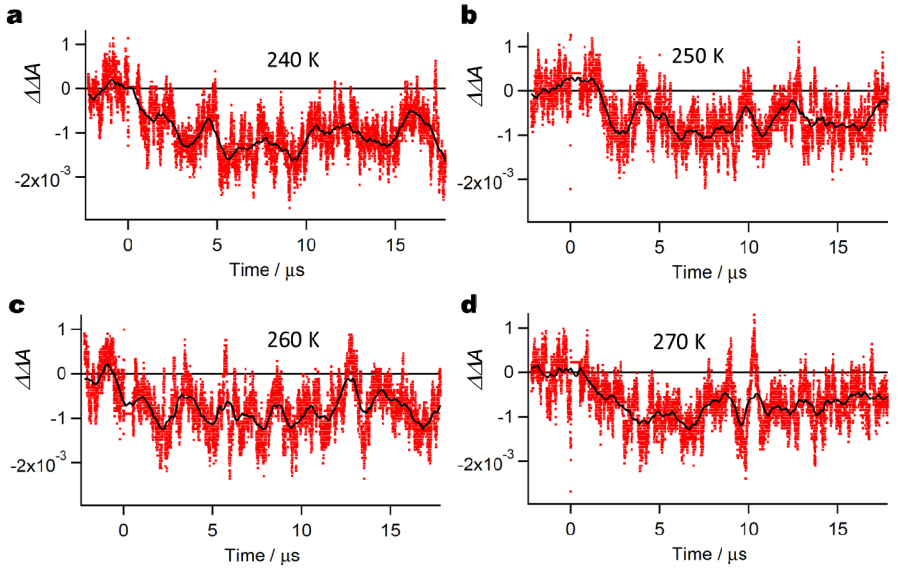

Fig. S4. Difference signals calculated from the data in Fig. S3: $\Delta\Delta A = \Delta A(28\ \text{mT}) - \Delta A(0)$. Red dots represent raw, unsmoothed data; black lines represent the same data after 1 μs boxcar smoothing.

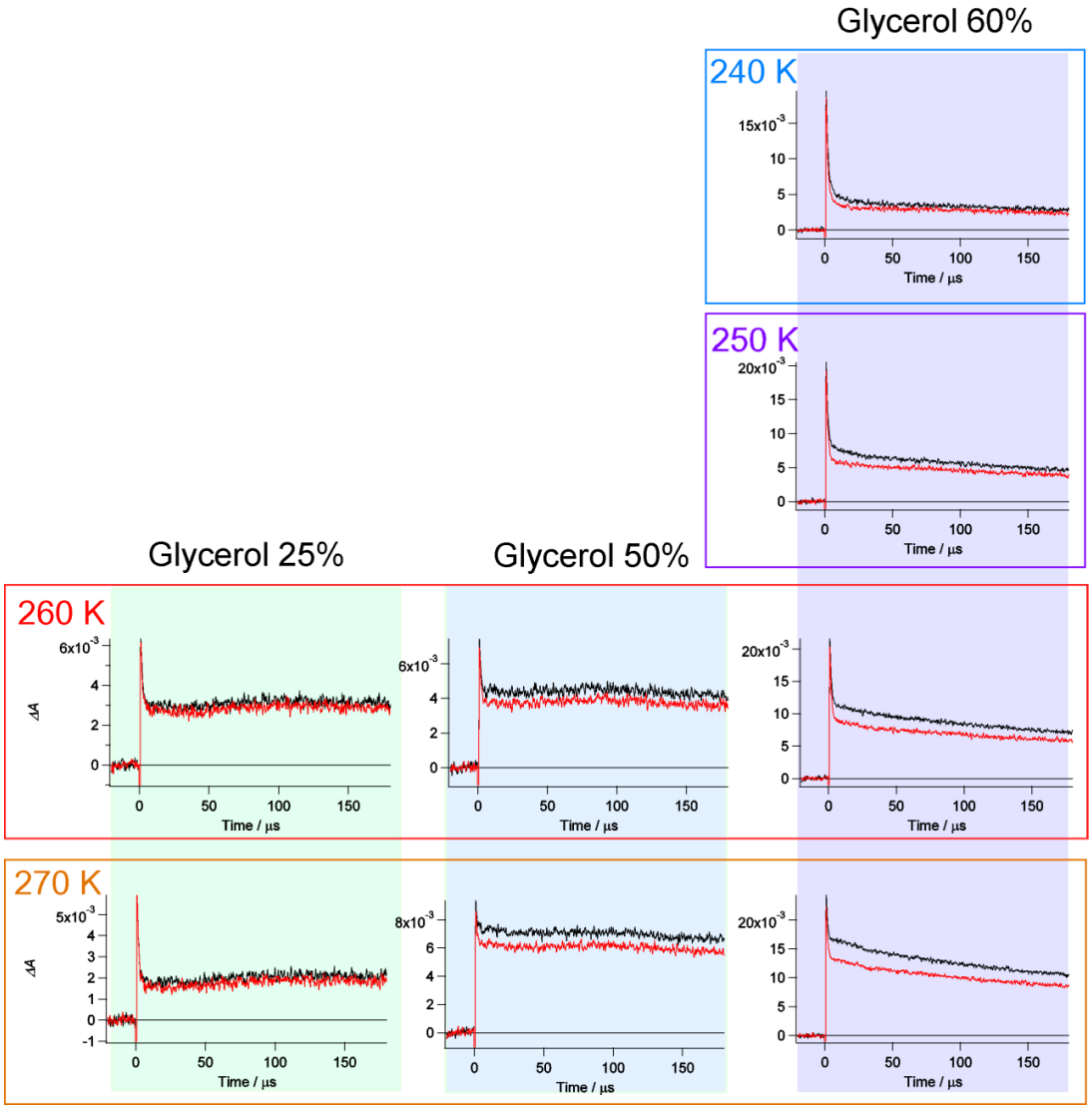

Fig. S5. Transient absorption kinetic time profiles of *At*Cry recorded at 510 nm in solutions of various water/glycerol composition and various temperatures with (red) and without (black) a 28 mT applied magnetic field. Results were obtained as the average of 10 laser shots, with 500 ns boxcar smoothing.

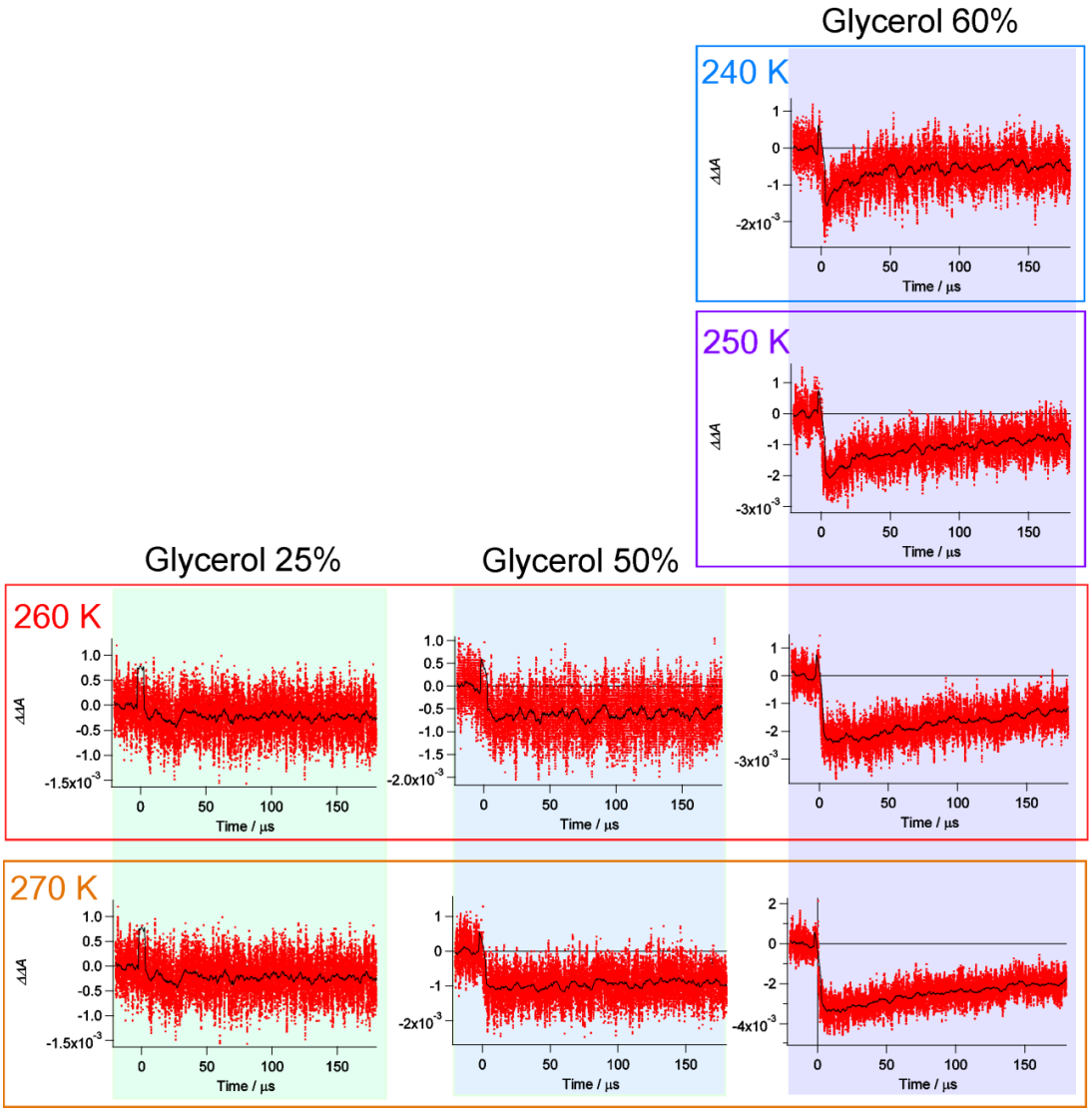

Fig. S6. Difference signals calculated from the data in Fig. S5: $\Delta\Delta A = \Delta A(28\ \text{mT}) - \Delta A(0)$. Red dots represent raw, unsmoothed data; black lines represent the same data after 5 μs boxcar smoothing.

2. Flavin–tryptophan photoreaction mechanism

Fig. 4 shows RP1 as formed in a *singlet* state from the photo-excited singlet state of the FAD cofactor (^{1}FAD*) in *At*Cry and *Ec*PL. Much of the photochemistry of free (i.e. not protein-bound) flavins proceeds from the photo-excited *triplet* state formed by intersystem crossing from the excited singlet. Although in principle possible in *At*Cry and *Ec*PL, this reaction pathway is excluded by the observation that an applied magnetic field of intensity exceeding the hyperfine interactions *reduces* the yield of RP2 (Figs 2 and 3) and correspondingly *increases* the proportion of RP1 that returns directly to the ground state (1). Direct formation of RP1 from ^{1}FAD*, rather than via ^{3}FAD* probably has the advantage of a larger quantum yield because intersystem crossing is likely to be slower than electron transfer and so would compete less effectively with other processes that quench ^{1}FAD*, e.g. fluorescence.

The conclusion that electron transfer along the Trp-triad chain proceeds via a singlet route is supported by observations of magnetic field effects from flavin–tryptophan reaction systems that are known to proceed through the *triplet* route. Photo-induced electron transfer between a free flavin and surface-exposed tryptophan residues in hen egg white lysozyme (Fig. S7) and the apo-form of garden warbler Cry-1a (Fig. S8) show, as expected, magnetic field effects with the opposite phase, i.e. an *increased* yield of long-lived radicals. Formation of spin-correlated radical pairs via a *singlet* pathway in DASH-type cryptochromes has also been demonstrated using time-resolved EPR spectroscopy (2, 3).

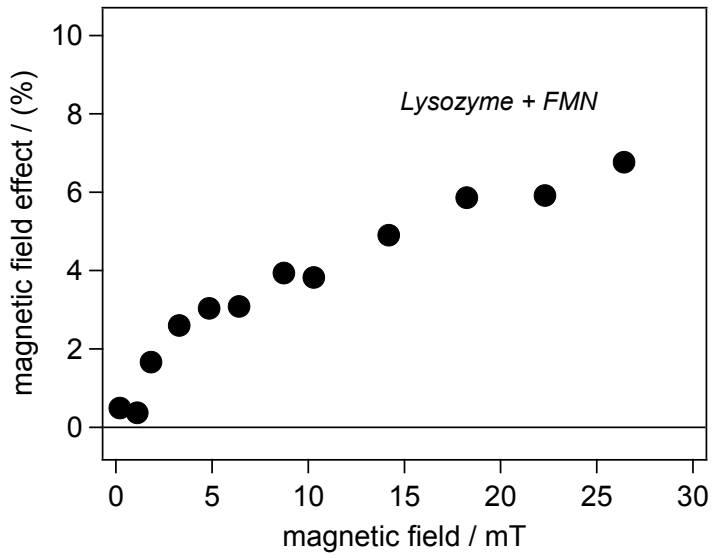

Fig. S7. Magnetic field effect on the yield of flavin mononucleotide (FMN) radicals formed by the intermolecular photochemical reaction of 200 μM FMN with 500 μM hen egg white lysozyme (data

reproduced from Ref (4)). The excited triplet state of the flavin undergoes electron transfer reactions with two solvent-exposed tryptophan residues (Trp-62 and Trp-123) on the surface of the protein (5).

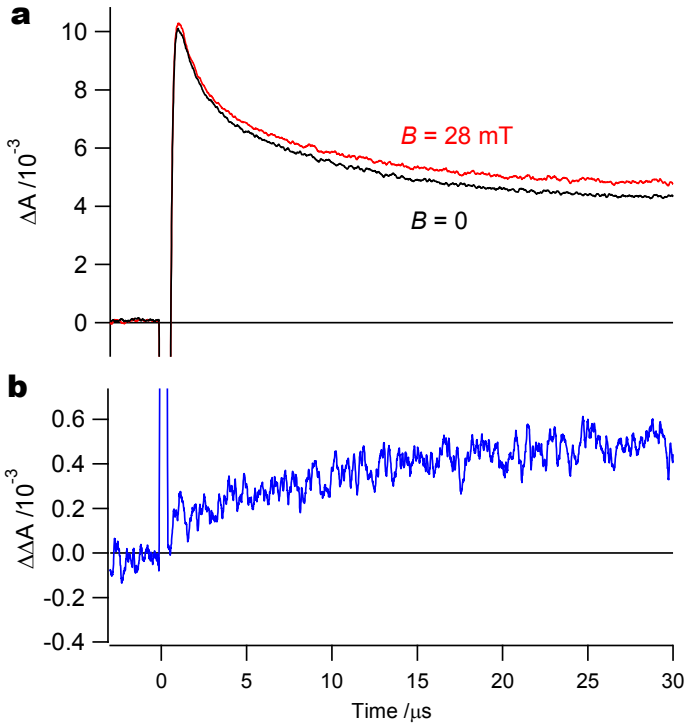

Fig. S8. Transient absorption kinetic time profiles of the intermolecular photochemical reaction of ~110 μM FAD with the apo form of ~110 μM garden warbler cryptochrome-1a, at 270 K, in ~50% glycerol solution, 20 mM HEPES buffer, 500 mM NaCl, pH 7.4. (**a**) Kinetic traces with and without a 28 mT magnetic field after 100 ns boxcar smoothing. (**b**) Difference signals calculated from the data in (a): $\Delta\Delta A = \Delta A(28\ \text{mT}) - \Delta A(0)$. The excited *triplet* state of the flavin undergoes electron transfer reactions with unknown solvent-exposed tryptophan and/or tyrosine residues on the surface of the protein.

3. Correlation between the magnetic field effect on the yield of RP2 and the lifetime of RP1 in *Ec*PL.

Table S1. *Ec*PL data plotted in Fig. 5

25% glycerol		
T / K	τ / μs	$\lvert MFE \rvert$ / %
265	1.7	5.5 ± 0.9
270	1.3	1.9 ± 0.5
275	1.6	2.8 ± 0.9

50% glycerol		
T / K	τ / μs	$\lvert MFE \rvert$ / %
235	7.4	14.0 ± 2.5
240	7.5	13.3 ± 2.2
	6.0	11.2 ± 1.4
245	6.6	9.9 ± 1.8
250	5.4	7.5 ± 1.9
	4.8	10.7 ± 1.0
255	4.6	9.6 ± 1.6
260	3.6	6.8 ± 1.1
	3.2	5.4 ± 0.7
265	3.1	6.6 ± 2.0
270	2.3	5.4 ± 1.4
	2.1	5.1 ± 0.6

65% glycerol		
T / K	τ / μs	$\lvert MFE \rvert$ / %
250	5.7	9.4 ± 1.6
260	4.6	10.4 ± 1.2
270	4.3	9.7 ± 2.1

τ is the lifetime of RP1 (measured at 600 nm) and $\lvert MFE \rvert$ is the absolute value of the magnetic field effect (measured at 510 nm) on the yield of RP2.

4. Calculation of $B_{1/2}$

Values of $B_{1/2}$ were calculated using the Weller equation (6):

$$B_{1/2} = \sqrt{3}\frac{\tilde{a}_{\mathrm{A}}^2 + \tilde{a}_{\mathrm{B}}^2}{\tilde{a}_{\mathrm{A}} + \tilde{a}_{\mathrm{B}}} \tag{1}$$

where A and B label the radicals and $\tilde{a}_{\mathrm{K}}$ is the effective hyperfine coupling (HFC) of radical K, given by (7):

$$\tilde{a}_{\mathrm{K}} = \sqrt{\frac{4}{3}\sum_i a_{i\mathrm{K}}^2 I_{i\mathrm{K}}(I_{i\mathrm{K}}+1)}\,. \tag{2}$$

$a_{i\mathrm{K}}$ and $I_{i\mathrm{K}}$ are the isotropic HFC and the spin quantum number of nucleus i in radical K[*]. Isotropic HFCs (Table S2) were calculated (by I. Kuprov) with Gaussian 03 using the UB3LYP/EPR-III level of theory. Lumiflavin was used as a proxy for FAD.

Table S2. Isotropic HFCs of $\mathrm{FAD}^{\bullet-}$ and $\mathrm{TrpH}^{\bullet+}$

$\mathrm{FAD}^{\bullet-}$	
	HFC / μT
N5	523.3
N6	188.7
N14	−3.5
N16	−38.3
H20	56.5
H21[a]	−141.6
H22[a]	−141.6
H23[a]	−141.6
H24	−387.2
H25[b]	439.9
H26[b]	439.9
H27[b]	439.9
H28[c]	0.0
H29[c]	407.0
H30[c]	407.0
H31	−18.9

$\mathrm{TrpH}^{\bullet+}$	
	HFC / μT
N6	146.5
N9	321.5
H16	−39.6
H17	−93.1
H18	1604.6
H19	45.7
H20	−10.4
H21	23.3
H22	−278.0
H23	−598.3
H24	−488.0
H25	−363.7
H26	−208.3
H27	−40.0

[*] The literature has conflicting definitions of the effective hyperfine coupling constant. We have chosen to use a definition incorporating a factor of 4/3 (Rodgers *et al*. *J. Am. Chem. Soc*. **129**, 6746-6755 (2007)). The version of Equation (1) given by Weller *et al*. has a leading factor of 2 instead of $\sqrt{3}$ because their version of Equation (2) does not contain the 4/3 factor.

[a] Average of values for H21, H22 and H23 to allow for internal rotation of methyl group.
[b] Average of values for H25, H26 and H27 to allow for internal rotation of methyl group.
[c] H29 and H30 represent the protons of the first methylene group of the ribityl chain in FAD. The HFC of H28 (9.9 μT) was set to zero.

The atom numbers in Table S2 are those assigned by the Gaussian calculation (see below)

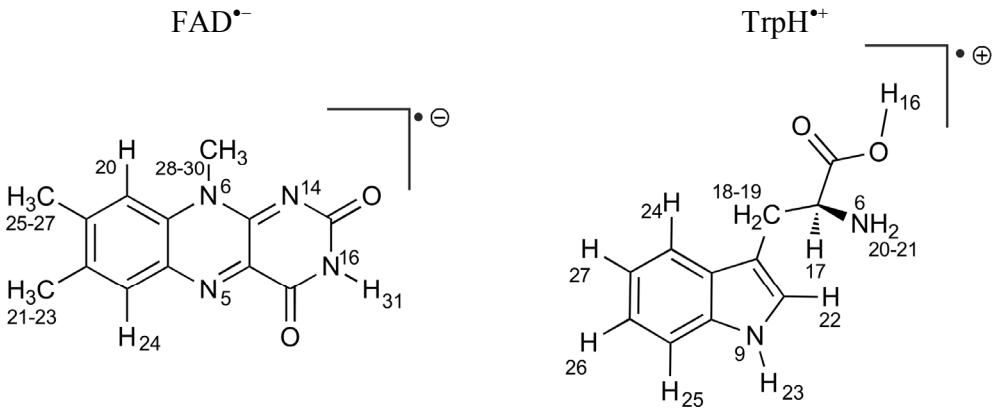

Using the data in Table S2, Equations (1) and (2) give $\tilde{a}_{\mathrm{FAD}}$ = 1.40 mT and $\tilde{a}_{\mathrm{Trp}}$ = 1.94 mT and hence $B_{1/2}$ = 2.97 mT.

Rodgers *et al.* have investigated the accuracy of Equation (1) using the exponential model (8, 9) in which radical pairs are assumed to recombine from the singlet and triplet states with the same rate constant, k (10). When $k << \tilde{a}_{\mathrm{K}}$ (K = A, B), Equation (1) was found to give an upper bound to the 'true' value of $B_{1/2}$ (determined by simulating the magnetic field dependence of the product yields). When $k \approx \tilde{a}_{\mathrm{K}}$, Equation (1) gives a good estimate of the 'true' value, and when $k >> \tilde{a}_{\mathrm{K}}$, it dramatically underestimates $B_{1/2}$. From the values of k_{f} and k_{b} reported in the text (1–5 × 10^5 s^{-1}) and the values of $\tilde{a}_{\mathrm{K}}$ quoted above (N.B. 1 mT ≈ 1.76 × 10^8 rad s^{-1}), it is clear that $k << \tilde{a}_{\mathrm{K}}$. The 'true' value of $B_{1/2}$ should therefore be smaller than the Weller value of $\sim 3\ \mathrm{mT}$. The experimental observation that $B_{1/2}$ ≈ 10–12 mT therefore strongly suggests the involvement of additional processes that broaden the magnetic field-dependence of the reaction yield.

5. Simulation of magnetic field effects

The magnetic field effects shown in Fig. 6 were calculated using the equation of motion of the radical pair spin density operator $\left|\rho(t)\right\rangle$ in Liouville space:

$$\frac{\mathrm{d}\left|\rho(t)\right\rangle}{\mathrm{d}t} = \left(-\mathrm{i}\hat{\hat{H}} + \hat{\hat{K}} + \hat{\hat{R}}\right)\left|\rho(t)\right\rangle \qquad (3)$$

The coherent and incoherent spin dynamics resulting from Zeeman and hyperfine interactions, chemical reactivity, and decoherence/relaxation processes were included by means of the superoperators $\hat{\hat{H}}$, $\hat{\hat{K}}$, and $\hat{\hat{R}}$ respectively.

The quantum yield of RP2 (Φ_{RP2}) was determined from Equation (3) using the *Spinach* spin dynamics package (11) with spin relaxation added as summarized below. *Spinach*'*s* zero-track elimination (ZTE) routine was used to reduce the dimension of the Liouvillian (12). A non-linear least squares fitting procedure (the *lsqnonlin.m* routine from the *Optimisation Toolbox* in MATLAB 2010b) was used to fit the calculated field-dependence of Φ_{RP2} to the experimental data. The background field experienced by the sample when no current flowed in the Helmholtz coils was assumed to be negligible.

Hamiltonian superoperator, $\hat{\hat{H}}$. The electron Zeeman interactions of the two radicals were assumed to be isotropic with identical g-values ($g = 2$). At the weak fields considered here, any effects of different g-values or of nuclear Zeeman interactions are negligibly small. It proved computationally impracticable to include more than 5 nuclear spins in the calculation (one ^{14}N and four ^{1}H with isotropic HFCs, giving a Liouvillian matrix with dimension 36,864 prior to ZTE and 6,930 after ZTE). The two largest HFCs in $\mathrm{TrpH}^{\bullet+}$ and the largest in $\mathrm{FAD}^{\bullet-}$ were included explicitly. The remaining HFCs in each radical were lumped together into a single spin-1/2 nucleus with an isotropic HFC (a') adjusted so that the correct value of $\tilde{a}_{\mathrm{K}}$ was obtained from Equation (2), see Table S3. The same HFCs were used for both proteins.

Table S3. HFCs used to calculate magnetic field effects

$\mathrm{FAD}^{\bullet-}$	
	HFC / μT
N5	523.3
a'	1106.5

$\mathrm{TrpH}^{\bullet+}$	
	HFC / μT
H18	1604.6
H23	−598.3
a'	915.7

Kinetic superoperator, $\hat{\hat{K}}$. The calculation was based on the reaction scheme in Fig. 4, ignoring the slow reactions that return RP2 to the ground state and assuming that RP1 is formed instantaneously at $t = 0$ in a pure singlet state. Spin-selective electron–hole recombination of the singlet radical pair (rate constant k_b) and spin-independent formation of RP2 from RP1 (rate constant k_f) were included by means of Haberkorn recombination operators unless otherwise stated (13).

Relaxation superoperator, $\hat{\hat{R}}$. Initial simulations were performed to investigate the magnetic responses of the $[\mathrm{FAD}^{\bullet-}\ \mathrm{TrpH}^{\bullet+}]$ radical pair in the absence of relaxation processes. k_f was fixed at $2.5\times10^5\ \mathrm{s}^{-1}$ (as described in the text), k_b was varied to cover the range $0.5 \le k_b / k_f \le 6$, and the quantum yield of RP2, $\Phi_{RP2}(B)$, was determined for magnetic fields, B, in the range $0 < B < 50\ \mathrm{mT}$. The percentage low and high field effects (LFE and HFE) were calculated as

$$\frac{\max[\Phi_{RP2}(B)] - \Phi_{RP2}(0)}{\Phi_{RP2}(0)} \times 100\% \quad \text{and} \quad \frac{\Phi_{RP2}(0) - \Phi_{RP2}(50\ \mathrm{mT})}{\Phi_{RP2}(0)} \times 100\% \qquad (4)$$

respectively, with the results shown in Fig. S9.

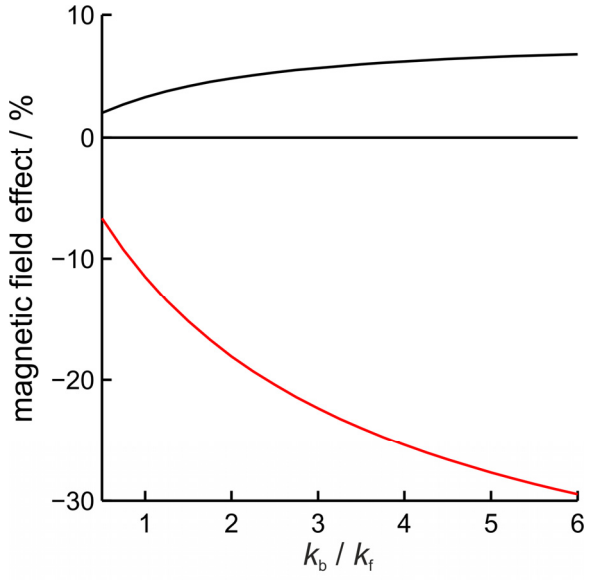

Fig. S9. Dependence on k_b / k_f of the calculated percentage LFE (black) and HFE (red) magnetic field effects for $[\mathrm{FAD}^{\bullet-}\ \mathrm{TrpH}^{\bullet+}]$ with $k_f = 2.5\times10^5\ \mathrm{s}^{-1}$, $k_{STD} = 0$.

These simulations indicate that the percentage magnetic field effect for the reaction scheme in Fig. 4 increases monotonically with k_b / k_f. The estimated values of k_b / k_f obtained for *At*Cry (~2.0) and *Ec*PL (~0.5) suggest a possible rationale for the larger magnetic response for *At*Cry (Fig. 6). Fig. S9 may also be used to rationalise the correlation between the magnetic field effect on *Ec*PL and the RP1 lifetime (Fig. 5). As the temperature is lowered and/or the glycerol content is increased, k_f decreases causing k_b / k_f to increase, predicting a larger magnetic response.

Attempts to fit the data in Fig. 6 without relaxation were not successful (Fig. S10). k_f was fixed at 2.5×10^5 s^{-1} (see text) and k_b was the only variable parameter. The values of k_b returned by the fitting procedure were 3.8×10^5 s^{-1} (*At*Cry) and 9.1×10^4 s^{-1} (*Ec*PL). Of the various relaxation/decoherence models summarized below, only singlet–triplet dephasing provided a satisfactory description of the data in Fig. 6.

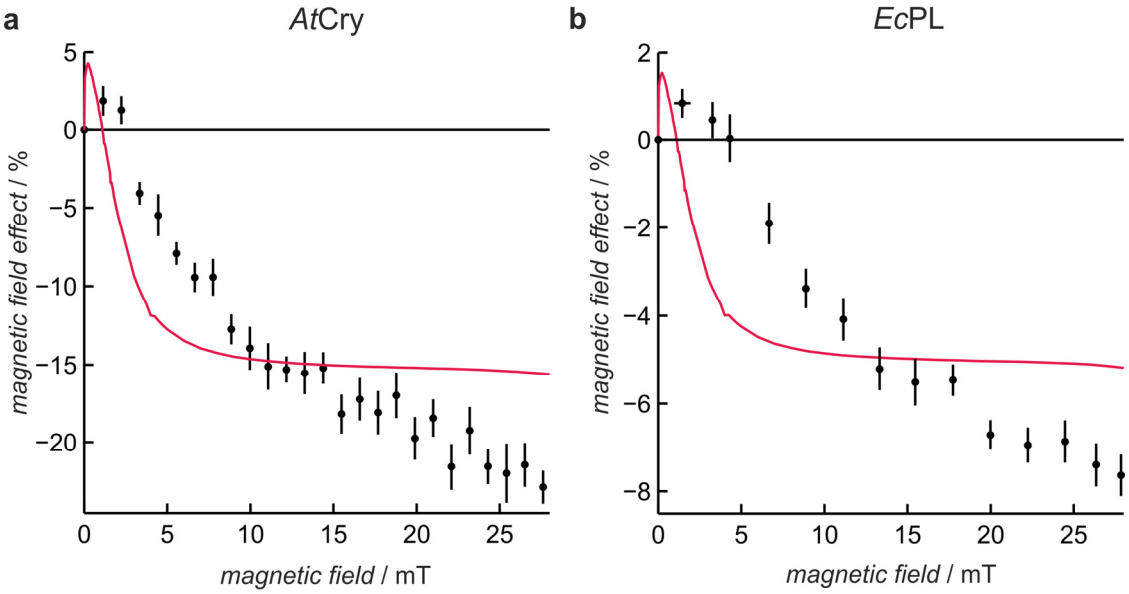

Fig. S10. The results of attempts to fit the data of Fig. 6 without including spin relaxation. (**a**) *At*Cry. (**b**) *Ec*PL.

Singlet–triplet dephasing was included by means of the phenomenological superoperator (14)

$$\hat{\hat{R}} = -k_{\mathrm{STD}} \sum_{q=0,\pm1} \left\{ \left|\mathrm{ST}_q\right\rangle\left\langle\mathrm{ST}_q\right| + \left|\mathrm{T}_q\mathrm{S}\right\rangle\left\langle\mathrm{T}_q\mathrm{S}\right| \right\} \qquad (5)$$

The results are described in the text. Agreements with the data (Fig. 6) of comparable quality were obtained with the three rate constants k_b, k_f, and k_{STD} scaled identically. Fixing the value of k_f as described in the text allowed a unique fit.

Modulation of anisotropic HFCs. Spin relaxation arising from modulation of anisotropic HFCs by isotropic rotational diffusion was included by means of Redfield theory (15, 16). The optimization variables were k_b, k_f and the rotational correlation time, τ_c. Restrictions on CPU time limited the calculation to three anisotropic HFCs (Table S4: Gaussian 03, UB3LYP/EPR-III), chosen for their large isotropic and anisotropic couplings.

Table S4. Selected anisotropic HFCs of $FAD^{\bullet-}$ and $TrpH^{\bullet+}$

		A_{jj} / μT	*Principal axes*[a]		
$FAD^{\bullet-}$	N5	−100.1	0.9581	−0.3068	0.0000
		−86.8	0.3068	0.9518	0.0000
		1756.9	0.0000	0.0000	1.0000
	H25	610.6	0.6882	0.0517	0.7237
		612.5	0.6968	−0.3254	−0.6393
		724.8	0.2024	0.9442	−0.2600
$TrpH^{\bullet+}$	H23	−1082.6	0.7540	0.6139	−0.2336
		−705.4	0.2344	0.0808	0.9688
		−6.9	−0.6136	0.7852	0.0830

[a]In the coordinate system used in the Gaussian output log file. Same atom numbering as in Table S2.

Phenomenological exponential relaxation was modelled as described by Bagryansky *et al*. (17) using time constants T_0 at zero-field, and T_1 and T_2 at high field. Both field-independent and field-dependent T_1 and T_2 parameters were investigated. In the latter case, the relaxation rate varied with the strength of the applied magnetic field, $\omega_0 = \gamma_e B_0$, and an adjustable correlation time, τ_c, as $\tau_c / (1 + \omega_0^2 \tau_c^2)$.

Lindblad master equation. Following Gauger *et al*. (18), relaxation induced by randomly fluctuating fields in three orthogonal directions was modelled using the Lindblad approach. The relaxation rates were assumed to have the form $\tau_c / (1 + \omega_0^2 \tau_c^2)$ where the correlation time τ_c was treated as a variable parameter.

Jones-Hore kinetic superoperator. The recently proposed alternative to the Haberkorn treatment of spin-selective recombination kinetics (13), which produces twice the singlet–triplet dephasing, was incorporated as described by Jones and Hore (19).

Averaging of anisotropic hyperfine interactions. Rotational diffusion in the viscous solutions used to obtain the data in Fig. 6 may not be sufficiently fast to average completely the anisotropic HFCs. Simulations were therefore performed without added relaxation, with spherical averaging over uniform distributions of radical pair orientations, using the HFC tensors in Table S4.

Various combinations of the above approaches were also explored.

References

1. Henbest KB*, et al.* (2008) Magnetic-field effect on the photoactivation reaction of *Escherichia coli* DNA photolyase. *Proc. Natl. Acad. Sci. USA* 105:14395-14399.
2. Weber S*, et al.* (2010) Origin of light-induced spin-correlated radical pairs in cryptochrome. *J. Phys. Chem. B* 114:14745-14754.
3. Biskup T*, et al.* (2011) Time-resolved EPR identifies unexpected electron transfer in cryptochrome. *Angew. Chem. Int. Ed.*:in press.
4. Miura T, Maeda K, Arai T (2003) Effect of coulomb interaction on the dynamics of the radical pair in the system of flavin mononucleotide and hen egg-white lysozyme (HEWL) studied by a magnetic field effect. *J. Phys. Chem. B* 107:6474-6478.
5. Hore PJ, Kaptein R (1983) Proton nuclear magnetic-resonance assignments and surface accessibility of tryptophan residues in lysozyme using photochemically induced dynamic nuclear-polarization spectroscopy. *Biochemistry* 22:1906-1911.
6. Weller A, Nolting F, Staerk H (1983) A quantitative interpretation of the magnetic-field effect on hyperfine-coupling-induced triplet formation from radical ion-pairs. *Chem. Phys. Lett.* 96:24-27.
7. Schulten K, Bittl R (1986) Probing the dynamics of a polymer with paramagnetic end groups by magnetic-fields. *J. Chem. Phys.* 84:5155-5161.
8. Brocklehurst B (1976) Spin correlation in geminate recombination of radical ions in hydrocarbons. 1. Theory of magnetic-field effect. *J. Chem. Soc. Faraday Trans. II* 72:1869-1884.
9. Kaptein R, Oosterhoff JL (1969) Chemically induced dynamic nuclear polarization II: (relation with anomalous ESR spectra). *Chem. Phys. Lett.* 4:195-197.
10. Rodgers CT, Norman SA, Henbest KB, Timmel CR, Hore PJ (2007) Determination of radical re-encounter probability distributions from magnetic field effects on reaction yields. *J. Am. Chem. Soc.* 129:6746-6755.
11. Hogben HJ, Krzystyniak M, Charnock GTP, Hore PJ, Kuprov I (2011) *Spinach* - a software library for simulation of spin dynamics in large spin systems. *J. Magn. Reson.* 208:179-194.
12. Kuprov I (2008) Polynomially scaling spin dynamics II: Further state-space compression using Krylov subspace techniques and zero track elimination. *J. Magn. Reson.* 195:45-51.

13. Haberkorn R (1976) Density matrix description of spin-selective radical pair reactions. *Mol. Phys.* 32:1491-1493.
14. Shushin AI (1991) The effect of the spin exchange interaction on SNP and RYDMR spectra of geminate radical pairs. *Chem. Phys. Lett.* 181:274-278.
15. Goldman M (2001) Formal theory of spin-lattice relaxation. *J. Magn. Reson.* 149:160-187.
16. Kuprov I (2011) Diagonalization-free implementation of spin relaxation theory for large spin systems. *J. Magn. Reson.* 209:31-38.
17. Bagryansky VA, Borovkov VI, Molin YN (2007) Quantum beats in radical pairs. *Russ. Chem. Rev.* 76:493-506.
18. Gauger EM, Rieper E, Morton JJL, Benjamin SC, Vedral V (2011) Sustained quantum coherence and entanglement in the avian compass. *Phys. Rev. Lett.* 106:040503.
19. Jones JA, Hore PJ (2010) Spin-selective reactions of radical pairs act as quantum measurements *Chem. Phys. Lett.* 488:90-93.